IQCH regulates spermatogenesis by interacting with CaM to promote the expression of RNA-binding proteins

Tiechao Ruan[1, 2]†, Ruixi Zhou[1, 2]†, Yihong Yang[3]†, Junchen Guo[4, 5], Chuan Jiang[1], Xiang Wang[1], Gan Shen[1], Siyu Dai[1], Suren Chen[6*], Ying Shen[1, 7*]

[1] Key Laboratory of Obstetrics, Gynecologic and Pediatric Diseases and Birth Defects of the Ministry of Education, Sichuan University, Chengdu, 610041, China;

[2] Department of Pediatrics, West China Second University Hospital, Sichuan University, Chengdu 610041 China;

[3] Reproduction Medical Center of West China Second University Hospital, Key Laboratory of Obstetric, Gynecologic and Pediatric Diseases and Birth Defects of Ministry of Education, Sichuan University, Chengdu 610041, China;

[4] Sichuan University-The Chinese University of Hong Kong (SCU-CUHK) Joint Laboratory for Reproductive Medicine, Key Laboratory of Obstetric, Gynaecologic and Paediatric Diseases and Birth Defects of Ministry of Education, West China Second University Hospital, Sichuan University, Chengdu 610041, China.

[5] Reproductive Endocrinology and Regulation Laboratory, Department of Obstetric and Gynaecologic, West China Second University Hospital, Sichuan University, Chengdu 610041, China.

[6] Education Key Laboratory of Cell Proliferation & Regulation Biology, College of Life Sciences, Beijing Normal University, Beijing 100875, China

[7] NHC Key Laboratory of Chronobiology, Sichuan University, Chengdu 610041, China;

†These authors contributed equally to this work

*Corresponding author:

Suren Chen

E-mail address: chensr@bnu.edu.cn;

Ying Shen

Phone: +86-15982083663.

E-mail address: yingcaishen01@163.com

Abstract

IQ motif-containing proteins can be recognized by calmodulin (CaM) and are essential for many biological processes. However, the role of IQ motif-containing proteins in spermatogenesis is largely unknown. In this study, we identified a loss-of-function mutation in the novel gene IQ motif-containing H (*IQCH*) in a Chinese family with male infertility, characterized by a cracked flagellar axoneme and abnormal mitochondrial structure. To verify the function of IQCH, *Iqch*-knockout mice were generated by CRISPR-Cas9 technology which reproduced the human phenotypes. Mechanistically, IQCH can bind to CaM and then regulate the expression of RNA-binding proteins (especially HNRPAB), which are indispensable for spermatogenesis. Collectively, this study firstly unveiled the function of IQCH, expanded the role of IQ motif-containing proteins in reproductive processes, and provided important guidance for genetic counseling and gene diagnosis for male infertility.

Introduction

Spermatogenesis is one of the most complex biological process in male organisms and functions to produce mature spermatozoa from spermatogonia in three phases: (i) spermatocytogenesis (mitosis), (ii) meiosis, and (iii) spermiogenesis (Hess and Renato de Franca 2008). This delicate process can be easily disturbed and further cause male reproductive disorders. Male infertility affects 7% of men in the general population, and its causes vary, ranging from anatomical or genetic abnormalities, systemic diseases, infections, trauma, iatrogenic injury, and gonadotoxins (Krausz et al. 2018). Approximately 10% of the human genome is related to reproductive processes; thus, male infertility is often predicted to be largely genetic in origin, whereas only 4% of infertile men are diagnosed with a distinct genetic cause (Krausz and Riera-Escamilla 2018). Genetic causes are highly heterogeneous and involve chromosomal abnormalities, point mutations in single genes, copy number variations, microRNA dysfunction, and polygenic defects (Meschede and Horst 1997, Traven et al. 2017). The highest percentage of known genetic factors that account for up to 25% of male infertility are karyotype anomalies, Y chromosome microdeletions, and *CFTR* mutations, which are mostly associated with azoospermia (Krausz and Riera-Escamilla 2018). However, in a relatively high proportion of infertile men (40%), the etiology cannot be recognized and is also referred to as idiopathic. With the help of assisted reproductive techniques (ART), some men have the chance to reproduce, however, there is a risk of passing on undetermined genetic abnormalities. In addition, genetic defects leading to fertilization failure and embryo development

arrest cannot be effectively rescued by ART; thus, discovering novel genetic factors and further confirming their molecular mechanisms are of clinical importance.

Calcium (Ca) is an essential element that acts as a universal intracellular second messenger. Ca is indispensable for many physiological processes in male reproduction, including spermatogenesis, sperm movement, capacitation, hyperactivation, acrosome reaction, chemotaxis, and fertilization (Valsa et al. 2015). Therefore, Ca deficiency is mentioned to be a main contributor to male infertility (Beigi Harchegani et al. 2019). Calmodulin (CaM) is defined as a major Ca sensor that activates many kinds of enzymes in response to an increase in intracellular Ca^{2+} by interacting with a diverse group of cellular proteins (Klee et al. 1980, Means et al. 1982). CaM binds to proteins through recognition motifs, including the short CaM-binding motif containing conserved Ile and Gln residues (IQ motif) for Ca^{2+}-independent binding and two related motifs for Ca^{2+}-dependent binding (Nie et al. 2009). The identified IQ motif-containing proteins include a good range of proteins with biological functions, one of which is sperm surface proteins, suggesting that IQ motif-containing proteins might play a potential role in male reproductive processes (Wen et al. 1999, Dolmetsch et al. 2001). Moreover, it has been revealed that CaM is predominantly expressed in the mammalian testis, from the pachytene to meiotic division stages (Smoake et al. 1974, Kakiuchi et al. 1982, YAMAMOTO 1985, Sano et al. 1987, Kägi et al. 1988, Moriya et al. 1995). However, limited IQ motif-containing proteins have been reported to be responsible for male fertility. It has been shown that the IQ motif-containing D (IQCD) is primarily accumulated in the acrosome area of

spermatids during mouse spermiogenesis, and the acrosome reaction was inhibited in human spermatozoa by anti-IQCD antibody, suggesting a potential function of IQCD in fertilization and the acrosome reaction (Zhang et al. 2019). Moreover, *Iqcf1* knockout (KO) male mice showed significantly less fertility, which was related to reduced sperm motility and acrosome reaction (Fang et al. 2015). Importantly, *Iqcg* is required for mouse spermiogenesis, which is attributable to its role in flagellar formation and/or function (Harris et al. 2014). Humans and mice without IQCN presented failed fertilization rates related to manchette assembly defects (Dai et al. 2022). Although reliable findings provide substantial clues for IQ motif-containing proteins participating in male reproductive processes, the relevant regulatory mechanism and the function of many other IQ motif-containing proteins in spermatogenesis have not been determined thus far.

Here, we revealed a testis-specific IQ motif containing H gene, *IQCH*, which is essential for spermiogenesis and fertilization. Disrupting IQCH leads to deficient acrosome action and abnormal structure of the axoneme and mitochondria in both humans and mice. Moreover, it is suggested that the interaction of IQCH and CaM is a prerequisite for IQCH function, which further regulates the expression of RNA-binding proteins (especially HNRPAB) during spermatogenesis. Collectively, our findings unveiled a novel genetic diagnostic indicator of male infertility, and the uncovered mechanism of IQCH in spermatogenesis might shed new light on the treatment of this disease.

Results

Identification of a novel homozygous variant of *IQCH* involved in male infertility

A 33-year-old man from a consanguineous family with primary infertility for four years was recruited in our study (Fig. 1A). Semen analysis of this patient revealed an inordinately decreasing sperm motility and count, as well as abnormal sperm morphology (Table 1). In addition to the proband, his great uncle was also affected, he had never conceived during sexual intercourse without contraception in his marriage. We further explored the possible genetic cause through whole-exome sequencing (WES) analysis, and a homozygous deletion variant in *IQCH* (c.387+1_387+10del, NM_0010317152) was identified in the proband. This variant is rare in the general human population according to the 1000 Genomes Project (0.007%), ExAC Browser (0.059%), and gnomAD databases (0.024%). We further clarified the putative contribution of this variant in this family by Sanger sequencing. Noticeably, this homozygous variant was affirmed in his infertile great-uncle, and the fertile parents of the proband carried the heterozygote of this variant (Fig. 1A).

Moreover, we used the minigene splicing assay to examine the effect of this variant on *IQCH* mRNA splicing. The electrophoresis results revealed that wildtype-*IQCH* (WT-*IQCH*) yielded one transcript with a size of 381 bp, whereas the mutant-*IQCH* (Mut-*IQCH*) resulted in one strong band of 263 bp (Fig. 1B, i). Sanger sequencing further showed that the variant resulted in the absence of the whole exon 4, which was expected to translate into a truncated protein (Fig. 1B, ii and iii). Therefore, we further constructed a plasmid containing the aberrant cDNA

sequence of *IQCH* caused by the splicing mutation to verify the effect of the variant on protein expression. The western blotting results showed that the Mut-c*IQCH* plasmid did not express IQCH while the WT-c*IQCH* plasmid did (Fig. 1B, iv). We further conducted immunofluorescence staining of spermatozoa from the proband and the control. We barely detected the expression of IQCH protein in the spermatozoa from the proband compared to the control (Fig. 1C). Taken together, these results reveal that this identified *IQCH* variant is responsible for the splicing abnormality and further causes the lack of IQCH expression, which is likely the genetic cause of male infertility in this family.

IQCH deficiency leads to sperm with cracked axoneme structures accompanied by defects in the acrosome and mitochondria

A comprehensive sperm morphology analysis was further conducted on the proband (the semen was not available from his great-uncle). Papanicolaou staining revealed that the spermatozoa displayed multiple flagellar morphological abnormalities, such as coiled, bent, irregular, and even fractured tails (Fig. 2A). These morphological anomalies were confirmed more precisely by scanning electron microscopy (SEM) analysis (Fig. 2B). Significantly, more subtle abnormalities, such as axoneme exposure, bending, and cracking, were further identified between the midpiece and the principal piece of the proband's spermatozoa (Fig. 2B). As expected, a deranged or incomplete '9+2' microtubule structure of the flagella was observed from the proband by transmission electron microscopy (TEM) analysis (fig. S1, A). In addition, we

detected ultrastructural defects in the spermatozoa nucleus, including irregular shape, large vacuoles, and deformed acrosomes (Fig. 2C). The mitochondria of the spermatozoa had an abnormal arrangement and enlarged diameter (Fig. 2C).

Moreover, we performed immunofluorescence staining for the marker of the acrosome (peanut agglutinin: PNA) as well as the mitochondrial marker (Transcription Factor A, Mitochondrial: TFAM) to confirm the deficiency of the acrosomes and mitochondria in the proband's spermatozoa. The results of the PNA and TFAM staining suggested that the spermatozoa acrosomes and mitochondria were severely defective in the proband compared to the control (Fig. 2, D and E). In addition, we performed SEPTIN4 (SEPT4) staining, a functional marker of the annulus, to explore whether the flagellar fracture at the joint between the middle piece and principal piece was caused by a nonfunctional annulus. The results showed that there was no significant difference in the SEPT4 signal of the spermatozoa between the proband and the control (fig. S1, B).

Impairment of male fertility in mice without *Iqch*

To further consolidate the role of IQCH in male reproduction, we first explored the pattern of *Iqch* expression in mice by quantitative real-time PCR (qPCR) and found that *Iqch* was predominantly expressed in the mouse testis compared to other organs (fig. S2, A). Additionally, we investigated the temporal expression of *Iqch* in mouse testes on different postnatal days. The results revealed that the expression of *Iqch* showed a significant increase on postnatal Day 21, peaked on postnatal Day 35, and

then presented stable expression (fig. S2, A). To better understand the role of IQCH during spermatogenesis, we performed immunofluorescence staining of the germ cells at different developmental stages in human and mouse testes. The exact localization of IQCH shared the same pattern in human and mouse spermatogenesis, being mainly detected in the cytoplasm of spermatocytes and round spermatids and the flagella of late spermatids (fig. S2, B and C). The testis-enriched expression of *Iqch*/IQCH suggested its potential role in spermatogenesis.

We next generated *Iqch* knockout (KO) mice using clustered regularly interspaced short palindromic repeat (CRISPR)-Cas9 technology. We used a guide RNA targeting exons 2 through 3 of *Iqch* to achieve the knockout (fig. S3, A). Polymerase chain reaction (PCR), reverse transcription-PCR (RT-PCR), and western blotting analysis further confirmed the success of the *Iqch* KO mouse construction (fig. S3, B). The *Iqch* KO mice showed no overt abnormalities in their development or behavior. The *Iqch* KO female mice showed normal fertility, and hematoxylin-eosin (H&E) staining further showed that the *Iqch* KO female mice had normal follicle development compared to the WT mice (fig. S3, C-E). However, the fertility of the KO male mice was significantly reduced compared to that of the WT mice, including a reduction in the pregnancy rate and litter size (Fig. S3, F). There was no detectable difference in the testis/body weight ratio between the WT and *Iqch* KO mice (fig. S3, G), and the histology of testes and epididymides in the *Iqch* KO mice showed no obvious abnormalities compared to the WT mice (fig. S4, A and B).

However, the results of the computer-assisted sperm analysis (CASA) affirmed

that sperm motility was significantly reduced in the KO mice, and the sperm count was slightly decreased (Table 2, Movie S1 and S2). Moreover, morphological anomalies of the sperm flagella were easily observed, such as an unmasking, bending, or cracking axoneme, which recapitulated the flagellar phenotype of the infertile patient (Fig. 3, A and B). We further found that during the spermatogenic process, the abnormality of axoneme exposure had already occurred when the spermatozoa flagellum developed (fig. S5, A). Intriguingly, tail defects, including bending and cracking between the middle piece and the principal piece, were mainly present in the epididymal spermatozoa (fig. S5, B), suggesting that more severe flagellum breakage might occur during sperm movement.

We further performed TEM analysis to investigate the ultrastructural defects in the testicular and epididymal spermatozoa of the *Iqch* KO mice. In contrast to the WT mice, the spermatozoa of the *Iqch* KO mice showed dilated intermembrane spaces of mitochondria and even loss of some mitochondrial material (Fig. 3C). However, the annulus did not present significant differences between the *Iqch* KO and WT mice (Fig. 3C), indicating that the disruptive link between the flagellar middle piece and the principal piece might result from mitochondrial defects but not the annulus. The immunofluorescence staining of the mitochondrial marker (Solute carrier family 25 member 4: SLC25A4) and SEPT4 also revealed that the mitochondria of the spermatozoa of the *Iqch* KO mice were severely defective, and there was no significant difference in the annulus of the spermatozoa between the *Iqch* KO mice and WT mice, which was consistent with the proband (fig. S6, A and B).

Poor in vitro fertilization (IVF) outcomes in the *Iqch* KO male mice

To evaluate the cause of the damaged fertility of the *Iqch* KO male mice, mature oocytes from WT female mice in their reproductive period were retrieved and placed into culture dishes with sperm from the *Iqch* KO mice and WT mice for IVF treatment. We found that 70% of the embryos had pronuclei in the WT group, while the fertilization rate of the *Iqch* KO group was dramatically reduced, accounting for 47% (Fig. 4A). Consequently, the rates of both two-cell embryos and blastocysts were significantly lower in the *Iqch* KO male mice than in the WT male mice (Fig. 4A). Noticeably, the inactive acrosome reaction was observed in most of the sperm from the *Iqch* KO mice (Fig. 4B), leading to the inability to cross the zona pellucida (fig. S7, A). Furthermore, abnormal acrosome development was evident in the testes of the *Iqch* KO mice using PNA staining (fig. S7, B). Similarly, the expression of PNA was abnormal in the mature sperm of the *Iqch* KO male mice (Fig. 4C). In the sperm and testis of the *Iqch* KO male mice and the proband, the PLCζ fluorescence signal was attenuated and abnormally localized (Fig. 4D, fig. S7, C and D). Taken together, these data suggested that *Iqch* might play an important role in the acrosomal formation, which is essential for fertilization.

RNA-binding proteins are the most relevant targets by which IQCH regulates spermatogenesis

To elucidate the molecular mechanism by which IQCH regulates male fertility, we

243 performed liquid chromatography tandem mass spectrometry (LC-MS/MS) analysis
244 using mouse sperm lysates and detected 288 interactors of IQCH (Data S1). Gene
245 Ontology (GO) analysis of the IQCH-bound proteins revealed many particular
246 enrichment pathways related to fertilization, sperm axoneme assembly, mitochondrion
247 organization, calcium channel, and RNA processing (Fig. 5A). Intriguingly, 33
248 ribosomal proteins were identified (Fig. 5B), indicating that IQCH might be involved
249 in protein synthesis. Using proteomic analysis on sperm from the *Iqch* KO mice, we
250 further assessed key proteins that might be activated by IQCH. A total of 1,993
251 differential proteins were quantified, including 807 upregulated proteins and 1,186
252 downregulated proteins (Fig. 5C). GO analysis revealed that the significantly
253 downregulated proteins were enriched in RNA processing, gene expression,
254 mitochondrion biogenesis, and calcium ion regulation (Fig. 5D), which was consistent
255 with the enrichment of the IQCH-bound proteins.

256 Importantly, the cross-analysis revealed that 76 proteins were shared between the
257 IQCH-bound proteins and the IQCH-activated proteins (Fig. 5E), implicating this
258 subset of genes as direct targets. Among the 76 proteins, 21 were RNA-binding
259 proteins (RBPs), 10 of which were suggested to be involved in spermatogenesis
260 (Kuroda et al. 2000, Yang et al. 2012, Chapman et al. 2013, Fukuda et al. 2013,
261 Legrand et al. 2019, Sechi et al. 2019, Liang et al. 2021, Tian and Petkov 2021, Wang
262 et al. 2022, Xu et al. 2022); 8 were involved in mitochondrial function; and 4 were
263 calcium channel activity-related proteins (Fig. 5F). We focused on SYNCRIP,
264 HNRNPK, FUS, EWSR1, ANXA7, SLC25A4, and HNRPAB, the loss of which

showed the greatest influence on the phenotype of the *Iqch* KO mice. Specifically, SYNCRIP, HNRNPK, FUS, EWSR1, and HNRPAB are RBPs that are linked to spermatogenesis by controlling mRNA translation or spermatid post-meiotic transcription (Kuroda et al. 2000, Fukuda et al. 2013, Sechi et al. 2019, Tian and Petkov 2021, Xu et al. 2022). ANXA7 is a calcium-dependent phospholipid-binding protein that is a negative regulator of mitochondrial apoptosis (Du et al. 2015). Loss of SLC25A4 results in mitochondrial energy metabolism defects in mice (Graham et al. 1997). We further confirmed the binding of IQCH between these proteins by the Co-IP assay (Fig. 6A) and substantiated their downregulation in the sperm of the *Iqch* KO mice by immunofluorescence staining and western blotting (Fig. 6B, fig. S8).

Among these interactors of IQCH, HNRPAB was the most significantly downregulated protein seen by proteomic analysis (Data S2), implying that HNRPAB might be the main target of IQCH. As an RBP, HNRPAB has been suggested to play an important role in spermatogenesis by regulating the translation of testicular mRNAs (Fukuda et al. 2013). We thus employed RNA-seq analysis using the sperm from the *Iqch* KO and WT mice to investigate the effects of RNA levels when IQCH is absent. Importantly, among the downregulated genes, most were related to male fertility, such as axoneme assembly, spermatid differentiation, flagellated sperm motility, and fertilization (fig. S9). We hypothesized that this downregulation is linked to HNRPAB binding. Considering the disrupted fertilization and axoneme assembly in the *Igch* KO mice, we chose the essential molecules involved in these two processes, including *Catsper1*, *Catsper2*, *Catsper3*, *Ccdc40*, *Ccdc39*, *Ccdc65*,

Dnah8, *Irrc6*, and *Dnhd1*, to confirm our speculation. We carried out RNA immunoprecipitation on formaldehyde cross-linked sperm followed by qPCR to evaluate the interactions between HNRPAB and *Catsper1*, *Catsper2*, *Catsper3*, *Ccdc40*, *Ccdc39*, *Ccdc65*, *Dnah8*, *Irrc6*, and *Dnhd1* in the KO and WT mice. As expected, the binding between HNRPAB and those important molecules was detected in the WT mice (Fig. 6C), supporting the functional role of HNRPAB in testicular mRNAs. Intriguingly, significantly decreased interactions between HNRPAB and those molecules were observed in the KO mice (Fig. 6C). Therefore, it is indicated that IQCH is involved in spermatogenesis by mainly regulating RBPs, especially HNRPAB, to further mediate essential mRNA expression in the testis.

The interaction of IQCH and CaM is a prerequisite for IQCH function

Given that IQCH is a calmodulin-binding protein, we hypothesized that IQCH regulates these key molecules by interacting with CaM (fig. S10, A and B). As expected, CaM interacted with IQCH, as indicated by LC-MS/MS analysis. We initially confirmed the binding of IQCH and CaM in the WT sperm by the Co-IP assay (Fig. 6D). In addition, their colocalization was detected during spermatogenesis by immunofluorescence staining (fig. S10, C).

We further confirmed the binding of IQCH and CaM in K562 cells, which express both IQCH and CaM (Fig. 6E). Moreover, a decrease in the expression of HNRPAB was observed when IQCH or CaM was knocked down (Fig. 6E, fig. S10D), suggesting that IQCH or CaM might regulate HNRPAB expression. We then

overexpressed IQCH and knocked down CaM or overexpressed CaM and knocked down IQCH in K562 cells, and found that the reduced HNRPAB expression could not be rescued in both two situations (Fig. 6F, fig. S10, E), indicating that CaM or IQCH cannot mediate HNRPAB expression alone. These findings suggested that the HNRPAB expression might be regulated by the interaction of IQCH and CaM.

We further confirmed that the IQ motif of IQCH is required for CaM binding using a microscale thermophoresis (MST) assay. The binding affinity between IQCH (target) from cell lysates overexpressing GFP-*IQCH* plasmids and recombinant CaM (ligand) was enhanced with increasing concentrations of recombinant CaM (Fig. 6G). However, their binding was disrupted when the IQ motif of IQCH was deleted (Fig. 6G). The Co-IP assay verified the above findings (Fig. 6H). Not surprisingly, the expression of HNRPAB in cells co-transfected with *IQCH* (△IQ) / *CaM* plasmids and control/ *CaM* plasmids was similar, but was lower than that in the cells overexpressing the WT-*IQCH* and *CaM* plasmids (Fig. 6H). Collectively, our findings suggest that IQCH interacts with CaM via IQ-motif to manipulate the expression of important molecules, especially HNRPAB, to play a role in spermatogenesis (Fig. 7).

Discussion

Throughout the evolution of divergent species, IQCH has been conserved, indicating its fundamental role in organisms. As a novel CaM-binding protein, IQCH was first identified in human and mouse testes and exclusively localized in spermatocytes and spermatids, suggesting its potential activity in spermatogenesis (Yin et al. 2005).

However, since IQCH was identified, no other findings have supported its function in male reproduction. In this study, we found that the mutation of *IQCH* impaired male fertility, including flagellar morphological abnormalities and axoneme cracking. Aberrant ultrastructure in sperm with the *IQCH* mutation was associated with severely defective acrosomes and mitochondria. Furthermore, *Iqch* KO mice showed similar irregularities in the flagellum, especially the axoneme and mitochondria. We also identified that *Iqch* KO mice displayed different degrees of functional defects in acrosomes. Thus, our work supported the vital role of IQCH in flagellar and acrosome development.

To date, only four IQ motif-containing proteins, including IQCD, IQCF1, IQCG, and IQCN, have been suggested to participate in spermatogenesis (Harris et al. 2014, Fang et al. 2015, Zhang et al. 2019, Dai et al. 2022). Most IQ motif-containing proteins function in Ca^{2+}dependent biological processes by binding to CaM (Chen et al. 2014, Harris et al. 2014, Fang et al. 2015); thus, IQCD, IQCF1, and IQCN are involved in fertilization and are relevant to the acrosome reaction, sperm capacitation, or manchette assembly (Fang et al. 2015, Zhang et al. 2019, Dai et al. 2022). In addition, because CaM has an impact on the actin cytoskeleton, *Iqcg* KO mice exhibit a detachment of sperm heads from tails (Harris et al. 2014). In our study, the *Iqch* KO mice also showed an impaired acrosome reaction, which caused reduced fertilization. Intriguingly, the axoneme breaks at the annulus and the mitochondrial defects were outstanding in the flagella of the *Iqch* KO mice, whose phenotypes were unexplored in the previously discovered IQ motif-containing proteins. Because CaM activation

can stimulate actin cytoskeleton changes, it is reasonable that flagellum formation is defective when IQCH is absent. Ca^{2+} is a key player in the regulation of mitochondrial functions (Bravo-Sagua et al. 2017). Thus, the absence of IQCH leads to a failed interaction with CaM and disrupts normal Ca^{2+} signaling, which consequently causes mitochondrial defects in *Iqch* KO mice and patients with *IQCH* variants. Our findings suggest that the fertilization function is the main action of IQ motif-containing proteins, while each specific IQ motif-containing protein also has its own distinct role in spermatogenesis.

However, there are few publications regarding the underlying mechanism of IQ motif-containing proteins manipulating reproductive processes, except for a recent study that stated that IQCN interacted with CaM to regulate the expression of CaM-binding proteins, including manchette-related proteins (LZTFL1, KIF27, and RSPH6A), IFT family proteins and their motor proteins (IFT22, IFT43, IFT74, IFT81, IFT140, IFT172, WDR19, TTC21B, and DYNC2H1), and ribosomal protein family proteins (RPS5, RPS25, RPS27, and RPSA) (Dai et al. 2022). In our study, it was observed that IQCH regulates the expression of RBPs by their interactions. RBPs are a large class of proteins that assemble with RNAs to form ribonucleoproteins (RNPs). RBPs function at various stages of RNA processing, including alternative splicing, RNA modification, nuclear export, localization, stability, and translation efficiency (Corley et al. 2020). RNA processing in male reproductive biology is essential for theproduction of mature sperm, and many RBPs have been demonstrated to be indispensable during spermatogenesis (Morgan et al. 2021). Among the RBPs,

HNRPAB, a heterogeneous nuclear RNP, showed the most significant reduction among the downregulated interactors of IQCH, suggesting that HNRPAB might be the most important downstream effector protein of IQCH. It has been reported that HNRPAB plays a central role in spermatogenesis by regulating stage-specific translation of testicular mRNAs (Fukuda et al. 2013). As expected, a RIP assay using an anti-HNRPAB antibody revealed binding between HNRPAB and the mRNAs of several important genes (*Catsper1*, *Catsper2*, *Catsper3*, *Ccdc40*, *Ccdc39*, *Ccdc65*, *Dnah8*, *Irrc6*, and *Dnhd1*) involved in spermatogenesis. We further found that the interaction of IQCH and CaM is a prerequisite for regulating HNRPAB expression. We thus hypothesized that IQCH regulates male fertility by binding to CaM and controls HNRPAB to manipulate the expression of key mRNAs involved in spermatogenesis.

In conclusion, our study identified a novel IQ motif-containing protein-coding gene, *IQCH*/*Iqch*, which is responsible for spermatogenesis in humans and mice, broadening the scope of known male infertility-associated genes thus further illustrating the genetic landscape of this disease. In addition, our study suggested an unexplored mechanism in which IQCH regulates the expression of key RBPs in spermatogenesis, especially HNRPAB, by interacting with CaM to play crucial roles in fertilization and axoneme assembly. We believe that our findings will provide genetic diagnostic markers and potential therapeutic targets for infertile males with *IQCH* pathogenic variants.

Materials and Methods.

Study participants

A male infertility family was recruited from West China Second University Hospital, and healthy Chinese volunteers were enrolled as controls. The study was conducted according to the tenets of the Declaration of Helsinki, and ethical approval was obtained from the Ethical Review Board of West China Second University Hospital, Sichuan University. Each subject signed an informed consent form.

WES and Sanger sequencing

Peripheral blood samples were obtained from all subjects, and genomic DNA was extracted using a QIAamp DNA Blood Mini Kit (QIAGEN, Germany; 51126). The exomes of the subject were captured by Agilent SureSelect Human All Exon V6 Enrichment kits (Agilent, CA, USA) and then sequenced on a HiSeq X-TEN system (Illumina, CA, USA). All reads were mapped to the human reference sequence (UCSC Genome Browser hg19) using Burrows-Wheeler Alignment. After quality filtration with the Genome Analysis Toolkit, functional annotation was performed using ANNOVAR through a series of databases, including the 1000 Genomes Project, dbSNP, HGMD, and ExAC. PolyPhen-2, SIFT, MutationTaster, and CADD were used for functional prediction. Variant verification of *IQCH* in patients was confirmed by Sanger sequencing using the primers listed in table S1.

Minigene assay

The minigene splicing assay was used to explore the effect of the *IQCH* variant (c.387+1_387+10del) on splicing. WT-*IQCH* and Mut-*IQCH* sequences, including intron 3, exon 4, and intron 4, were PCR-amplified separately from the genomic DNA of the control and patient. The two amplified fragments were cloned into the minigene vector pSPL3 between the EcoRI and BamHI sites through the Basic Seamless Cloning and Assembly Kit (TransGen Biotech, China, CU201-02). After transfection into HEK293T cells by DNA and siRNA transfection reagent (Polypus, France, 101000046), the splicing patterns of the transcripts produced from the WT-*IQCH* and Mut-*IQCH* plasmids were analyzed by RT-PCR, gel electrophoresis, and Sanger sequencing. The primers used for the plasmid genomic amplification and the RT-PCR are listed in table S1.

Iqch knockout mice

The animal experiments were approved by the Experimental Animal Management and Ethics Committee of West China Second University Hospital, Sichuan University. All animal procedures complied with the Animal Care and Use Committee of Sichuan University. The mouse *Iqch* gene has 6 transcripts and is located on chromosome 9. According to the structure of the *Iqch* gene, exons 2~3 of the *Iqch-201* (ENSMUST00000042322.10) transcript were recommended as the knockout region. The region contains a 215 bp coding sequence, and deletion of this region was expected to disrupt IQCH protein function. The sgRNA sequences, synthesized by Sangon Biotech (Shanghai, China), are listed in table S2. The two complementary

DNA oligos of each sgRNA target were annealed and ligated to the pUC57-sgRNA plasmid (Addgene, USA) for cloning. The recombinant plasmid was transformed into DH5α competent cells, and the positive clone was screened based on kanamycin resistance and sequencing. The recombinant plasmid was linearized and purified by phenol-chloroform extraction. Transcriptions of the sgRNAs *in vitro* were performed using the MEGAshortscript Kit (Ambion, USA, AM1354) and purified using the MEGAclear Kit (Ambion, USA, AM1908). Cas9 mRNA was purchased from TriLink BioTechnologies. The mouse zygotes were co-injected with the RNA mixture of Cas9 mRNA (~50 ng/μl) and sgRNA (~30 ng/μl). The injected zygotes were transferred into pseudopregnant recipients to obtain the F0 generation. DNA was extracted from the tail tissues of the 7-day-old offspring, and PCR amplification was carried out with genotyping primers. A stable F1 generation (heterozygous mice) was obtained by mating the positive F0 generation mice with wild-type C57BL/6JG-pt mice. Primers used for the genotyping are listed in table S2.

Mouse fertility testing

To confirm the fertility of the *Iqch* KO male mice, natural mating tests were conducted. Briefly, three *Iqch* KO and three littermate control sexually mature male mice (8-12 weeks old) were paired with two 6- to 8-week-old normal C57BL/6J females (each male was mated with two female mice) for 6 months. The vaginal plugs of the mice were examined every morning. Female mice with vaginal plugs were fed separately, and the number of pups per litter was recorded.

IVF

Eight-week-old C57BL/6J female mice were superovulated by injecting 5 IU of pregnant mare serum gonadotropin (PMSG), followed by 5 IU of human chorionic gonadotropin (hCG) 48 h later. Sperm was released from the cauda epididymis of 10-week-old male mice, and sperm capacitation was performed for 50 min using a test-yolk buffer with HEPES (TYH) solution. The cumulus-oocyte complexes (COCs) were obtained from the ampulla of the uterine tube 14 h after the hCG injection. The ampulla was torn with a syringe needle, and the COCs were gently squeezed onto liquid drops of a human fallopian tube fluid (HTF) medium. The COCs were then incubated with ~5 μl of the sperm suspension in HTF liquid drops at 37 °C under 5% CO_2. After 6 h, the eggs were washed several times using an HTF medium to remove the cumulus cells and then transferred to liquid drops of a potassium simplex optimized medium(KSOM).

Acrosome reaction analysis

The spermatozoa were collected from the cauda epididymis and capacitated for 50 min in a TYH medium at 37 °C under 5% CO_2. Highly motile sperm were collected from the upper portion of the medium, and 10 μM of calcium ionophore A23187 (Sigma-Aldrich, CA, USA, C7522) was added to induce the acrosome reaction. After 15 min, the spermatozoa were spotted on a glass microscope slide, dried, and fixed with 4% paraformaldehyde (PFA) for 10 min. The acrosomes were stained with

Coomassie brilliant blue staining.

H&E staining

For the staining of the testicular tissues, samples were dissected from the adult mice and fixed in 4% PFA overnight at 4 °C. The fixed tissues were embedded in paraffin, sectioned (5 μm thick), dewaxed, and rehydrated. The sections of the testis were stained with hematoxylin and an eosin solution (Beyotime, Shanghai, China, C0105M) before imaging using a microscope (Leica, Germany).

Immunofluorescence staining

For sperm immunostaining, fresh sperm samples were fixed with 4% PFA for 20 min at room temperature. For the staining of the testis tissues, heat-induced antigen retrieval was performed in a citrate antigen retrieval solution (Beyotime, Shanghai, China, P0081) according to the manufacturer's requirements. After permeabilization with 1% Triton X-100 for 30 min, the sperm slides were blocked with 5% bovine serum albumin serum for 1 h at room temperature. Primary antibodies were added to the slide and incubated overnight at 4 °C. After washing three times with PBS, the slides were incubated with secondary antibodies for 1 h at room temperature. The nuclei were counterstained with DAPI dye (Sigma□Aldrich, CA, USA, 28718-90-3) and mounted with an antifade mounting medium. Images were captured with a laser-scanning confocal microscope (Olympus, Japan). Detailed information on the antibodies is provided in table S3.

qPCR

Total RNA was extracted from the mouse testes using an RNA Easy Fast Tissue/Cell Kit (Tiangen Biotech, China, 4992732). Approximately 0.3 mg of total RNA was converted into cDNA with the PrimeScript RT Reagent Kit (Takara, Japan, RR037A) according to the manufacturer's instructions. The cDNAs were individually diluted 10-fold to be used as templates for the subsequent qPCR with iTaq Universal SYBR Green Supermix (Bio-Rad Laboratories, USA, 1725124). Mouse *Gapdh* was used as an internal control. The mRNA expression of detected targets was quantified according to the $2^{-\Delta\Delta Ct}$ method. The primers used for the qPCR are listed in table S1 and table S2.

Papanicolaou staining

Semen samples were fixed in 4% paraformaldehyde, and the coated slides were air-dried before being rehydrated with 80%, 70%, and 50% ethanol and distilled water. The samples were then stained with Lea's hematoxylin, rinsed with distilled water, and stained with G-6 orange stain and EA-50. Following the staining, the slides were dehydrated with ethanol and mounted.

SEM

The spermatozoa were fixed in 2.5% phosphate-buffered glutaraldehyde (GA) (Zhongjingkeyi Technology, Beijing, China) at room temperature for 30 min and then

deposited on coverslips. The coverslips were dehydrated via an ascending gradient of 50%, 70%, 95%, and 100% ethanol and air-dried. The specimens were then attached to specimen holders and coated with gold particles using an ion sputter coater before being viewed with a JSM-IT300 scanning electron microscope (JEOL, Tokyo, Japan).

TEM

Precipitation of the spermatozoa was fixed with 2.5% (vol/vol) glutaraldehyde in a 0.1 M phosphate buffer (PB) (pH 7.4), washed two times in PB, and two times in ddH_2O. Then, the tissues were immersed in 1% (wt/vol) OsO_4 and 1.5% (wt/vol) potassium ferricyanide aqueous solution at 4 °C for 2 h. After washing, the samples were dehydrated through graded alcohol (30%, 50%, 70%, 80%, 90%, 100%, 10 min each) in pure acetone (10 min twice). The samples were then infiltrated in a graded mixture (3:1, 1:1, 1:3) of acetone and SPI-PON812 resin (21 ml SPO-PON812, 13 ml DDSA and 11 ml NMA), and then the pure resin was changed. The specimens were embedded in pure resin with 1.5% BDMA and polymerized for 12 h at 45 °C and 48 h at 60 °C. The ultrathin sections (70 nm thick) were sectioned with a microtome (Leica EM UC6, Germany), double-stained with uranyl acetate and lead citrate, and examined by a transmission electron microscope (TECNAI G2 F20, Philips, USA).

Proteomic quantification

Proteins were extracted from the sperm samples using a radioimmunoprecipitation assay buffer (RIPA) lysis buffer (Applygen, Beijing, China, C1053) containing 1 mM

phenylmethanesulfonyl fluoride (PMSF) and protease inhibitors on ice. The supernatants were collected following centrifugation at 12,000 × g for 20 min. Protein concentrations were calculated by Bradford quantification and sodium dodecyl sulfate polyacrylamide gel electrophoresis (SDS-PAGE). An enzyme solution at a ratio of 1:20 of trypsin enzyme (μg) to substrate protein (μg) was added to 100 μg of the protein samples, vortexed, centrifuged at low speed for 1 minute, and incubated at 37 °C for 4 h. The peptide liquid obtained after salt removal was freeze-dried. The peptide sample was dissolved in 0.5 M TEAB and added to the corresponding iTRAQ labeling reagent and stored at room temperature for 2 h. The Shimadzu LC-20AB liquid phase system was used for purification, and the separation column was a 5 μm 4.6 × 250 mm Gemini C18 column for liquid phase separation of the sample. The dried peptide samples were reconstituted with mobile phase A (2% can, 0.1% FA) and centrifuged at 20,000 × g for 10 min, and the supernatant was taken for injection. The separation was performed by UltiMate 3000 UHPLC (Thermo Fisher). The sample was first enriched in a trap column and desalted and then entered into a self-packed C18 column. The peptides separated by the liquid phase chromatography were ionized by a nanoESI source and then passed to a tandem mass spectrometer Q-Exactive HF X (Thermo Fisher) for DDA (Data Dependent Acquisition) mode detection. The raw data were converted to mgf files for bioinformatics analysis, and protein identification from tandem mass spectra was performed by database searching (UniProt). The protein quantification process includes the following steps: protein identification, tag impurity correction, data normalization, missing value imputation, protein ratio

calculation, statistical analysis, and results presentation. Proteins with a 1.5-fold change and a p-value (using Student's *t*-test) less than 0.05 were defined as differentially expressed proteins.

RNA sequencing

Total RNA (~1 μg) was isolated from fresh spermatozoa from the WT mice (n=3) and the *Iqch* KO mice (n=3) using the RNAsimple Total RNA Kit (Tiangen Biotech, China, 4992858). A Ribo-Zero™ rRNA Removal Kit (MRZPL1224, llumina) was used to remove rRNA from the samples. RNA integrity was evaluated using the Agilent 2100 Bioanalyzer system (Agilent Technologies). An mRNA sequencing library for the RNA-seq was constructed using the TruSeq RNA Library Prep kit v2 (RS-122-2001, Illumina), followed by paired-end (2 × 100 bp) sequencing using the Illumina HiSeq 4000 Sequencing System (Illumina) at the Beijing Genomics Institute. Raw paired-end reads were filtered by FASTX-Toolkit. The quality of the reads was confirmed by FastQC (ver: 0.11.3). The raw data (raw reads) in the fastq format were processed through in-house Perl scripts. Feature Counts (ver: l.5.0-p3) were used to count the read numbers mapped to each gene. The fragments per kilobase million (FPKM) of each gene was calculated based on the length of the gene and the read count mapped to the gene. Signaling pathway matching analysis for the differentially expressed gene (DEG) list was performed using Kyoto Encyclopedia of Genes and Genomes (KEGG) Mapper (https://www.genome.jp/kegg/). The mapping of GO to DEGs was carried out using Blast2GO (ver: 4.1.9).

Western blotting and Co-IP

Proteins were extracted from the cultured cells and mouse testes using a RIPA lysis buffer containing 1 mM PMSF and protease inhibitors (Applygen, Beijing, China, P1265) on ice. The supernatants were collected following centrifugation at 12,000 × g for 20 min. The proteins were electrophoresed in 10% SDS-PAGE gels and transferred to nitrocellulose membranes (GE Healthcare). The blots were blocked in 5% milk and incubated with primary antibodies overnight at 4 °C, followed by incubation with anti-rabbit or anti-mouse IgG heavy and light chain(H&L) (horseradish peroxidase, HRP) (Abmart, Shanghai, China, M21002 and M21001) at a 1/10,000 dilution for 1 h. The signals were evaluated using a Super ECL Plus Western Blotting Substrate (Applygen, Beijing, China, P1050) and a Tanon-5200 Multi chemiluminescence imaging system (Tanon, Shanghai, China).

For the Co-IP assays, the extracted proteins were incubated with primary antibodies overnight at 4 °C. The lysates were then incubated with 20 μl of Pierce™ Protein A/G-conjugated Agarose for 2 h at room temperature. The beads were washed with a washing buffer [50 mM Tris-HCl (pH 7.4), 0.1% Triton X-100, and 500 mM NaCl], eluted with a 1.2×SDS loading buffer, and boiled for 5 min at 95 °C. Finally, the products were separated using SDS-PAGE and analyzed using immunoblotting procedures. Detailed information on the antibodies used in the western blotting experiments is provided in table S3.

Antibody production

The peptide used for raising the anti-IQCH antibody was derived from amino acid residues 406–435 (KAEAATKIQATWKSYKARSSFISYRQKKWA) of mouse IQCH. The peptide coupled with keyhole limpet hemocyanin (KLH) (Sigma-Aldrich, USA, H7017) was dissolved in saline, emulsified with 1 ml of Freund's complete adjuvant (Beyotime, China, P2036), and injected at multiple sites on the back of New Zealand white rabbits. The antiserum was collected within 2 weeks after the final injection.

Cell culture and transfection

We purchased the K562 cells (CRL-3344) and the HEK293T cells (CRL-11268) from the American Type Culture Collection. The K562 cell line is a human leukemia cell line showing a high expression levels of IQCH and CaM, and is used for the knockdown experiments. The K562 cells were cultured in Basic Roswell Park Memorial Institute 1640 Medium (Gibco, USA, C11875500BT) supplemented with 10% fetal bovine serum (Gibco, USA, 12483020). The HEK293T cells were cultured in Dulbecco's Modified Eagle Medium (Gibco, USA, 11965092) supplemented with 10% fetal bovine serum (Gibco, USA, 12483020). The expression plasmids, including pcDNA3.1-Flag-*CALM2*, pCMV-MCS-3* flag-WT-*IQCH,* and pCMV-MCS-3* flag-*IQCH(*△IQ*)*, and small interfering RNAs (siRNAs) of *CALM2* and *IQCH* were constructed by Vigene Biosciences (Jinan, China). The target sequences of siRNA are listed in table S1. The plasmids and siRNA were transfected into cells with a

jetPRIME transfection reagent (Polypus, France, 101000046) according to the manufacturer's protocol.

MST assay

The MST experiments were conducted on a Monolith NT.115 system (NanoTemper Technologies, Germany). Lysates of the HEK293T cells transfected with fluorescent GFP-*IQCH* or GFP-*IQCH*(△IQ) were normalized by raw fluorescence (count), diluted using an MST buffer (50 mM Tris-HCl pH 7.5, 150 mM NaCl, 10 mM MgCl2, 0.05% (v/v) Tween 20), and added to 16 PCR tubes (10 μl per tube). Then, the purified CaM was diluted using an MST buffer into 16 gradients. Ten microliters of different concentrations of CaM were mixed with 10 μl of fluorescent GFP-IQCH protein and GFP-*IQCH*(△IQ) and reacted in a dark box for 15 min at room temperature. The samples were added to monolith capillaries (NanoTemper, MO-L022) and subsequently subjected to MST analysis. The measurement protocol times were as follows: fluorescence before 5 sec, MST on 30 sec, fluorescence after 5 sec, delay 25 sec. The dissociation constant (Kd) was determined using a single-site model to fit the curve.

Statistical analysis

Data were compared for statistical significance using GraphPad Prism version 9.0.0 (GraphPad Software). The unpaired, two-tailed Student's t-test was used for the statistical analyses. The data are presented as the mean ± SEM, and statistically

significant differences are represented as *$p<0.05$.

References

Beigi Harchegani, A., A. Irandoost, M. Mirnamniha, H. Rahmani, E. Tahmasbpour and A. Shahriary (2019). "Possible Mechanisms for The Effects of Calcium Deficiency on Male Infertility." Int J Fertil Steril **12**(4): 267-272.

Bravo-Sagua, R., V. Parra, C. López-Crisosto, P. Díaz, A. F. Quest and S. Lavandero (2017). "Calcium Transport and Signaling in Mitochondria." Compr Physiol **7**(2): 623-634.

Chapman, K. M., H. M. Powell, J. Chaudhary, J. M. Shelton, J. A. Richardson, T. E. Richardson and F. K. Hamra (2013). "Linking spermatid ribonucleic acid (RNA) binding protein and retrogene diversity to reproductive success." Mol Cell Proteomics **12**(11): 3221-3236.

Chen, L. T., W. X. Liang, S. Chen, R. K. Li, J. L. Tan, P. F. Xu, L. F. Luo, L. Wang, S. H. Yu, G. Meng, K. K. Li, T. X. Liu, Z. Chen and S. J. Chen (2014). "Functional and molecular features of the calmodulin-interacting protein IQCG required for haematopoiesis in zebrafish." Nat Commun **5**: 3811.

Corley, M., M. C. Burns and G. W. Yeo (2020). "How RNA-Binding Proteins Interact with RNA: Molecules and Mechanisms." Mol Cell **78**(1): 9-29.

Dai, J., Q. Li, Q. Zhou, S. Zhang, J. Chen, Y. Wang, J. Guo, Y. Gu, F. Gong, Y. Tan, G. Lu, W. Zheng and G. Lin (2022). "IQCN disruption causes fertilization failure and male infertility due to manchette assembly defect." EMBO Mol Med **14**(12): e16501.

Dolmetsch, R. E., U. Pajvani, K. Fife, J. M. Spotts and M. E. Greenberg (2001). "Signaling to the nucleus by an L-type calcium channel-calmodulin complex through the MAP kinase pathway." Science **294**(5541): 333-339.

Du, Y., Y. Huang, Y. Gao, B. Song, J. Mao, L. Chen, L. Bai and J. Tang (2015). "Annexin A7

687 modulates BAG4 and BAG4-binding proteins in mitochondrial apoptosis." Biomed
688 Pharmacother **74**: 30-34.
689 Fang, P., W. Xu, D. Li, X. Zhao, J. Dai, Z. Wang, X. Yan, M. Qin, Y. Zhang, C. Xu, L. Wang and
690 Z. Qiao (2015). "A novel acrosomal protein, IQCF1, involved in sperm capacitation and the
691 acrosome reaction." Andrology **3**(2): 332-344.
692 Fukuda, N., T. Fukuda, J. Sinnamon, A. Hernandez-Hernandez, M. Izadi, C. S. Raju, K.
693 Czaplinski and P. Percipalle (2013). "The transacting factor CBF-A/Hnrnpab binds to the
694 A2RE/RTS element of protamine 2 mRNA and contributes to its translational regulation during
695 mouse spermatogenesis." PLoS Genet **9**(10): e1003858.
696 Graham, B. H., K. G. Waymire, B. Cottrell, I. A. Trounce, G. R. MacGregor and D. C. Wallace
697 (1997). "A mouse model for mitochondrial myopathy and cardiomyopathy resulting from a
698 deficiency in the heart/muscle isoform of the adenine nucleotide translocator." Nat Genet **16**(3):
699 226-234.
700 Harris, T. P., K. J. Schimenti, R. J. Munroe and J. C. Schimenti (2014). "IQ motif-containing G
701 (Iqcg) is required for mouse spermiogenesis." G3 (Bethesda) **4**(2): 367-372.
702 Hess, R. A. and L. Renato de Franca (2008). "Spermatogenesis and cycle of the seminiferous
703 epithelium." Adv Exp Med Biol **636**: 1-15.
704 Kägi, U., J. G. Chafouleas, A. W. Norman and C. W. Heizmann (1988). "Developmental
705 appearance of the Ca2+-binding proteins parvalbumin, calbindin D-28K, S-100 proteins and
706 calmodulin during testicular development in the rat." Cell Tissue Res **252**(2): 359-365.
707 Kakiuchi, S., S. Yasuda, R. Yamazaki, Y. Teshima, K. Kanda, R. Kakiuchi and K. Sobue
708 (1982). "Quantitative determinations of calmodulin in the supernatant and particulate fractions

709 of mammalian tissues." J Biochem **92**(4): 1041-1048.

710 Klee, C. B., T. H. Crouch and P. G. Richman (1980). "Calmodulin." Annu Rev Biochem **49**:
711 489-515.

712 Krausz, C., F. Cioppi and A. Riera-Escamilla (2018). "Testing for genetic contributions to
713 infertility: potential clinical impact." Expert Rev Mol Diagn **18**(4): 331-346.

714 Krausz, C. and A. Riera-Escamilla (2018). "Genetics of male infertility." Nat Rev Urol **15**(6):
715 369-384.

716 Kuroda, M., J. Sok, L. Webb, H. Baechtold, F. Urano, Y. Yin, P. Chung, D. G. de Rooij, A.
717 Akhmedov, T. Ashley and D. Ron (2000). "Male sterility and enhanced radiation sensitivity in
718 TLS(-/-) mice." Embo j **19**(3): 453-462.

719 Legrand, J. M. D., A. L. Chan, H. M. La, F. J. Rossello, M. L. Änkö, F. V. Fuller-Pace and R. M.
720 Hobbs (2019). "DDX5 plays essential transcriptional and post-transcriptional roles in the
721 maintenance and function of spermatogonia." Nat Commun **10**(1): 2278.

722 Liang, J., Y. Zheng, W. Zeng, L. Chen, S. Yang, P. Du, Y. Wang, X. Yu and X. Zhang (2021).
723 "Comparison of proteomic profiles from the testicular tissue of males with impaired and normal
724 spermatogenesis." Syst Biol Reprod Med **67**(2): 127-136.

725 Means, A. R., J. S. Tash and J. G. Chafouleas (1982). "Physiological implications of the
726 presence, distribution, and regulation of calmodulin in eukaryotic cells." Physiol Rev **62**(1):
727 1-39.

728 Meschede, D. and J. Horst (1997). "The molecular genetics of male infertility." Mol Hum
729 Reprod **3**(5): 419-430.

730 Morgan, M., L. Kumar, Y. Li and M. Baptissart (2021). "Post-transcriptional regulation in

731 spermatogenesis: all RNA pathways lead to healthy sperm." Cell Mol Life Sci **78**(24):
732 8049-8071.
733 Moriya, M., K. Fujinaga, M. Yazawa and C. Katagiri (1995). "Immunohistochemical localization
734 of the calcium/calmodulin-dependent protein phosphatase, calcineurin, in the mouse testis: its
735 unique accumulation in spermatid nuclei." Cell Tissue Res **281**(2): 273-281.
736 Nie, D., X. Yang and Z. Yankai (2009). "Molecular cloning and expression profile analysis of a
737 novel mouse testis-specific expression gene mtIQ1." Mol Biol Rep **36**(5): 1203-1209.
738 Sano, M., A. S. Ohshima, N. Kawamura, S. Kitajima and A. Mizutani (1987).
739 "Immunohistochemical study of calmodulin in developing mouse testis." J Exp Zool **241**(1):
740 51-59.
741 Sechi, S., A. Frappaolo, A. Karimpour-Ghahnavieh, M. Gottardo, R. Burla, L. Di Francesco, E.
742 Szafer-Glusman, E. Schininà, M. T. Fuller, I. Saggio, M. G. Riparbelli, G. Callaini and M. G.
743 Giansanti (2019). "Drosophila Doublefault protein coordinates multiple events during male
744 meiosis by controlling mRNA translation." Development **146**(22): dev183053.
745 Smoake, J. A., S. Y. Song and W. Y. Cheung (1974). "Cyclic 3',5'-nucleotide
746 phosphodiesterase. Distribution and developmental changes of the enzyme and its protein
747 activator in mammalian tissues and cells." Biochim Biophys Acta **341**(2): 402-411.
748 Tian, H. and P. M. Petkov (2021). "Mouse EWSR1 is crucial for spermatid post-meiotic
749 transcription and spermiogenesis." Development **148**(11): dev199414.
750 Traven, E., A. Ogrinc and T. Kunej (2017). "Initiative for standardization of reporting genetics
751 of male infertility." Syst Biol Reprod Med **63**(1): 58-66.
752 Valsa, J., K. P. Skandhan, P. S. Khan, K. P. Avni, S. Amith and M. Gondalia (2015). "Calcium

and magnesium in male reproductive system and in its secretion. I. Level in normal human semen, seminal plasma and spermatozoa." Urologia **82**(3): 174-178.

Wang, X. L., J. M. Li and S. Q. Yuan (2022). "Characterization of the protein expression and localization of hnRNP family members during murine spermatogenesis." Asian J Androl 25(3):314-321.

Wen, Y., R. T. Richardson and G. O'Rand M (1999). "Processing of the sperm protein Sp17 during the acrosome reaction and characterization as a calmodulin binding protein." Dev Biol **206**(2): 113-122.

Xu, H., J. Guo, W. Wu, Q. Han, Y. Huang, Y. Wang, C. Li, X. Cheng, P. Zhang and Y. Xu (2022). "Deletion of Hnrnpk Gene Causes Infertility in Male Mice by Disrupting Spermatogenesis." Cells **11**(8) 1277.

YAMAMOTO, N. J. A. h. e. c. (1985). "Immunoelectron microscopic localization of calmodulin in guinea pig testis and spermatozoa." **18**(2): 199-211.

Yang, F., Q. Wei, R. S. Adelstein and P. J. Wang (2012). "Non-muscle myosin IIB is essential for cytokinesis during male meiotic cell divisions." Dev Biol **369**(2): 356-361.

Yin, L. L., J. M. Li, Z. M. Zhou and J. H. Sha (2005). "Identification of a novel testis-specific gene and its potential roles in testis development/spermatogenesis." Asian J Androl **7**(2): 127-137.

Zhang, P., W. Jiang, N. Luo, W. Zhu and L. Fan (2019). "IQ motif containing D (IQCD), a new acrosomal protein involved in the acrosome reaction and fertilisation." Reprod Fertil Dev **31**(5): 898-914.

Acknowledgments: We thank the patient and the family members for their support

during this research study.

Competing interests: The authors declare that they have no competing interests.

Author contributions: Y.S. designed and supervised the study experiments. Y.Y. collected data and conducted the clinical evaluations. T.R., R.Z., and Y.S. performed experiments and analyzed most of the data. S.C. generated the CRISPR mice. J.G., C.J., X.W., G.S. and S.D. performed cell experiments. Y.S. wrote the manuscript with input from others. All authors revised and approved the article.

Ethics Approval and Consent to Participate: For human participants, this study was performed in line with the principles of the Declaration of Helsinki. Approval was granted by Ethics Committee of the Second West China Hospital of Sichuan University. Informed consent was obtained from all individual participants included in the study. For the animal experiments, they were performed in accordance with the recommendation of the Guide for the Care and Use of Laboratory Animals of the National Institutes of Health and the animal experiments were approved by the Experimental Animal Management and Ethics Committee of West China Second University Hospital (IACUC no. 2021(070)).

Funding: This study was funded by the National Key Research and Development Project (2019YFA0802101)

Data and materials availability: All data needed to evaluate the conclusions in the paper are present in the paper and/or the Supplementary Materials.

Figure legends

Fig. 1. Identification of a homozygous splicing mutation in *IQCH* in a consanguineous family with male infertility. (A) Pedigree analysis of the consanguineous family with two infertile males (II-1 and IV-1), with the black arrow pointing to the proband. The affected males exhibited the homozygous variant in *IQCH* by Sanger sequencing. Sequence chromatograms are shown below the pedigree. **(B)** (i) The electrophoresis results of the minigene assay show a decrease in the molecular weight of the RT-PCR products generated from the Mut-*IQCH* (263 bp) compared with the WT-*IQCH* (381 bp). (ii) Sanger sequencing of the complementary DNA of the splicing mutation showing the deletion of exon 4 in *IQCH*. (iii) The pattern diagram demonstrating the splicing effects caused by the *IQCH* mutation. (iv) Western blotting results showed that the Mut–c*IQCH* plasmids did not express IQCH. NC, negative control. Three independent experiments were performed. **(C)** Immunofluorescence staining showed that the expression of IQCH was barely detected in the proband's sperm compared with the control (blue, DAPI; green, α-Tubulin; red, IQCH; scale bars, 5 μm).

Fig. 2. Abnormal flagellar morphology and defective acrosomes and mitochondria in the infertile patient. (A and **B)** The Papanicolaou staining (A) and scanning electron microscopy (SEM) (B) results showed flagellar morphological abnormalities (scale bars in A, 5 μm; scale bars in B, 2.5 μm). The dotted boxes and red arrowheads denote the axoneme cracking and exposure. **(C)** Transmission electron

microscopy (TEM) results showing the deformed acrosomes and abnormal arrangement and diameter mitochondria (scale bars, 500 nm). The red arrowheads denote the abnormal mitochondria. N, nucleus; M, mitochondria. **(D** and **E)** Defects of the acrosome and mitochondria were observed in the proband's sperm by PNA (D) and TFAM (E) staining (blue, DAPI; green, α-Tubulin; red, PNA or TFAM; scale bars, 5 μm). PNA, peanut agglutinin; TFAM, Transcription Factor A, Mitochondrial.

Fig. 3. The absence of *Iqch* impaired spermatogenesis in mice. (A and **B)** The Papanicolaou staining (B) and SEM (C) results showing unmasking, bending, or cracking axoneme in the spermatozoa from the *Iqch* KO mice (n = 3 biologically independent WT mice and KO mice; scale bars in B, 5 μm; scale bars in C, 2.5 μm). The red arrowheads point to the axoneme abnormalities. **(C)** TEM revealing dilated intermembrane spaces of mitochondria and a normal annulus in the testicular and epididymal spermatozoa from the *Iqch* KO mice (n = 3 biologically independent WT mice and KO mice; scale bars, 500 nm). The red arrowheads point to the dilated intermembrane spaces of mitochondria. The green arrowheads point to the normal annulus. M, mitochondria.

Fig. 4. Poor IVF treatment outcomes from using sperm from the *Iqch* KO mice. (A) Representative pronucleus embryos, two-cell embryos, and blastocysts obtained from the WT mice and the *Iqch* KO mice. Significantly reduced fertilization rates, cleavage rates, and blastocyst formation rates were observed in the *Iqch* KO mice

compared to the WT mice (n = 3 biologically independent WT mice and KO mice; scale bars, 100 μm; Student's t test; *p < 0.05; error bars, s.e.m). **(B)** The acrosome reaction rates in the capacitated spermatozoa from the WT mice and *Iqch* KO mice were determined by Coomassie brilliant blue staining. The acrosome reaction rates were reduced in the spermatozoa from the *Iqch* KO mice (n = 3 biologically independent WT mice and KO mice; scale bars, 5 μm; Student's t-test; *p < 0.05; error bars, s.e.m). The green arrowheads indicate the reacted acrosomes. The red arrowheads indicate intact acrosomes. (**C** and **D**) PNA (C) and PLCζ (D) staining showing the abnormal acrosome morphology and aberrant PLCζ location and expression in the spermatozoa from the *Iqch* KO mice (n = 3 biologically independent WT mice and KO mice; scale bars, scale bars, 5 μm). The dotted box indicates the typical pattern of the PLCζ location and expression in the spermatozoa from the WT mice. PNA, peanut agglutinin; PLCζ, phospholipase C zeta 1.

Fig. 5. IQCH bound and activated male reproduction-related proteins in the sperm of the mice. (A) Bubble plots of the GO analysis showing that the IQCH-interacting proteins are significantly enriched in spermatogenesis and RNA processing in three categories: biological process, cellular component, and molecular function. GO, gene ontology. **(B)** Thirty-three ribosomal proteins interacted with IQCH in the sperm from the mice. **(C)** A heatmap showing the differential protein results from the proteomic analysis of the sperm from the WT and *Iqch* KO mice. **(D)** Bubble plots showing the decreased enrichment of proteins related to the

spermatogenetic process and RNA processing according to the GO analysis of the *Iqch* KO mice compared to the WT mice. **(E)** Venn diagram depicting the 76 overlapping proteins between the 1186 downregulated proteins in the sperm from the *Iqch* KO mice and the 288 proteins binding with IQCH. **(F)** Chord diagram showing 21 proteins involved in RNA binding, 8 proteins involved in mitochondrial function, and 4 proteins involved in calcium channel activity among the 76 overlapping proteins. HNRPAB showed the greatest reduction of expression in the *Iqch* KO mice.

Fig. 6. IQCH interacted with CaM to regulate the expression of HNRPAB and spermatogenesis. (A) A Co-IP assay of the mouse sperm lysates revealed that the seven proteins most relevant to the phenotype of the *Iqch* KO mice bound with IQCH. **(B)** Western blotting showing the reduced expression of the seven proteins in the sperm from the *Iqch* KO mice compared to the WT mice. **(C)** qPCR analysis of RNA immunoprecipitation (RIP) using HNRPAB antibodies and IgG antibodies on the mouse sperm lysates showed that HNRPAB interacted with several RNAs associated with fertilization and axoneme assembly. The qPCR analysis of RIP performed on the sperm lysates from the *Iqch* KO mice revealed a decrease in the interaction between HNRPAB and the RNA targets compared to the WT mice (Student's t-test; $*p < 0.05$; error bars, s.e.m). **(D)** The Co-IP assay showed the binding of IQCH and CaM in the WT sperm. **(E)** The Co-IP assay showed that the decreased expression of HNRPAB was due to the reduced binding of IQCH and CaM by the knockout of IQCH or CaM. **(F)** The overexpression of IQCH and the simultaneous knockout of CaM or the

overexpression of CaM and the simultaneous knockout of IQCH in K562 cells further confirmed that the downregulation of HNRPAB was due to the diminished interaction between IQCH and CaM by western blotting analysis. **(G)** Analysis of the binding affinity between GFP-IQCH from the cell lysates (target) and recombinant CaM (ligand) by a microscale thermophoresis (MST) assay showing the interaction between IQCH and CaM. Their interaction was destroyed after the deletion of the IQ motif within IQCH. **(H)** The Co-IP assay of the HEK 293 cells co-transfected with WT-*IQCH* and WT-*CaM* plasmids , co-transfected with *IQCH* (△IQ) and WT-*CaM* plasmids, or co-transfected with control and WT-*CaM* plasmids showed that CaM interacted with the IQ motif. The downregulation of HNRPAB was due to the disrupted interaction between IQCH and CaM. Three independent experiments were performed.

Fig.7. Proposed model for the mechanisms of action underlying the involvement of IQCH in spermatogenesis. IQCH interacts with CaM by IQ motif to regulate the expression of RNA binding proteins. RNA binding proteins, particularly HNRPAB, bind and regulate several RNAs that influence the development of acrosome, mitochondria, and axoneme, thereby playing a critical role in spermatogenesis.

Table 1: Results of the semen analysis and sperm morphology examination of the patient

Parameter	Patient	Reference*
Sperm volume, ml	2.8	≥1.5
Sperm concentration, million/ml	10.0	≥15
Vitality, %	30	≥58
Motility, %	4	≥32
Abnormal morphology (%)	99.5	-

*: The reference values were based on the guidelines provided in the WHO manual 5th edition (2010).

Table 2. Semen analysis using CASA in the mouse model of *Iqch* KO

	Adult Male Mice		
	WT	**KO**	**P[b] value**
Semen parameters			
Sperm concentration (10^6 /ml) [a]	94.51±10.68	67.75±3.70	0.038
Motility (%)	57.08±2.18	5.49±3.25	<0.001
Progressive motility (%)	57.00±2.05	5.49±3.25	<0.001
Sperm locomotion parameters			
Curvilinear velocity (VCL) (μm/s)	78.29±6.23	9.94±4.03	<0.001
Straight-line velocity (VSL) (μm/s)	36.18±2.09	2.90±1.98	<0.001
Average path velocity (VAP) (μm/s)	45.10±0. 19	4.17±2.49	<0.001
Amplitude of lateral head displacement (ALH) (μm)	0.77±0. 02	0.13±0.03	<0.001
Linearity (LIN)	0.46±0.01	0.27±0.08	0.047
Wobble (WOB, = VAP/VCL)	0.58±0.04	0.40±0.08	0.033
Straightness (STR, = VSL/VAP)	0.80±0.05	0.67±0.07	0.069
Beat-cross frequency (BCF) (Hz)	4.33±0.19	0.65±0.26	<0.001

[a] Epididymides and vas deferens, [b] two-tailed Student's t-test

n = 3 biologically independent WT mice or KO mice

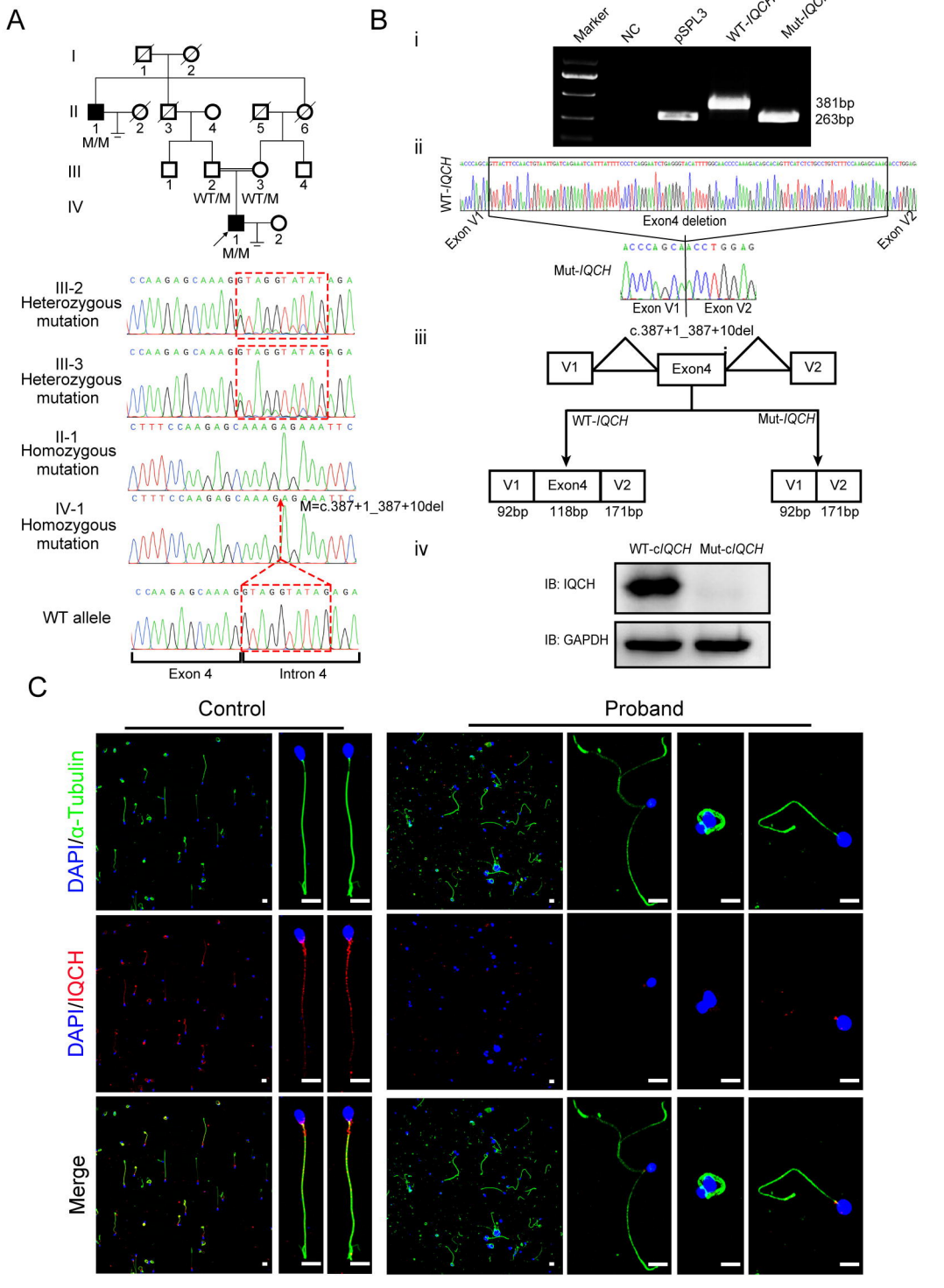
A
I
II
III
IV
M/M
WT/M
WT/M
M/M
III-2
Heterozygous
mutation
III-3
Heterozygous
mutation
II-1
Homozygous
mutation
IV-1
Homozygous
mutation
M=c.387+1_387+10del
WT allele
Exon 4
Intron 4
B
i
Marker
NC
pSPL3
WT-IQCH
Mut-IQCH
381bp
263bp
ii
WT-IQCH
Exon V1
Exon4 deletion
Exon V2
Mut-IQCH
Exon V1
Exon V2
iii
c.387+1_387+10del
V1
Exon4
V2
WT-IQCH
Mut-IQCH
V1
Exon4
V2
92bp
118bp
171bp
V1
V2
92bp
171bp
iv
WT-cIQCH
Mut-cIQCH
IB: IQCH
IB: GAPDH
C
Control
Proband
DAPI/α-Tubulin
DAPI/IQCH
Merge

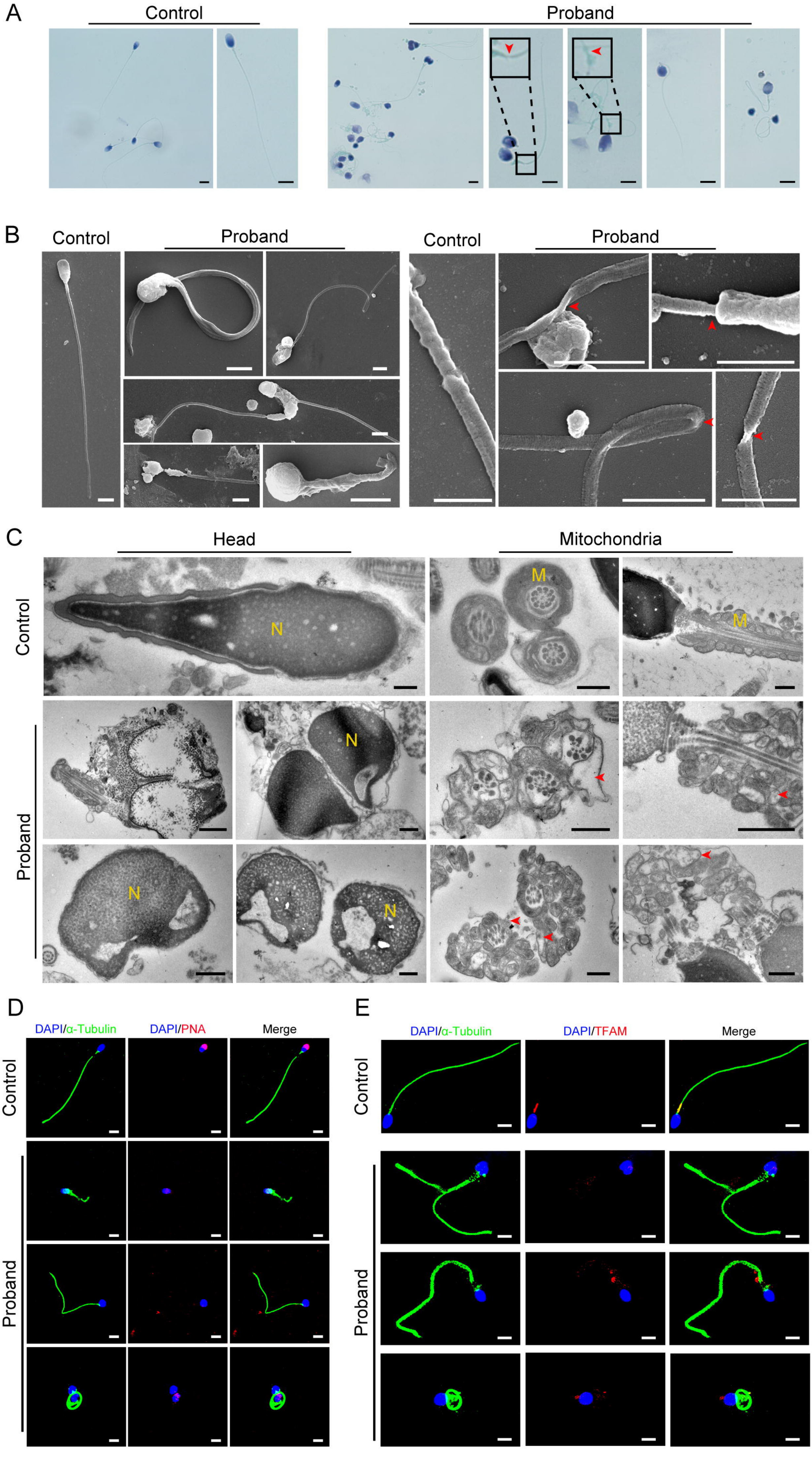
A
Control
Proband
B
Control
Proband
Control
Proband
C
Head
Mitochondria
Control
Proband
N
M
D
DAPI/α-Tubulin
DAPI/PNA
Merge
Control
Proband
E
DAPI/α-Tubulin
DAPI/TFAM
Merge
Control
Proband

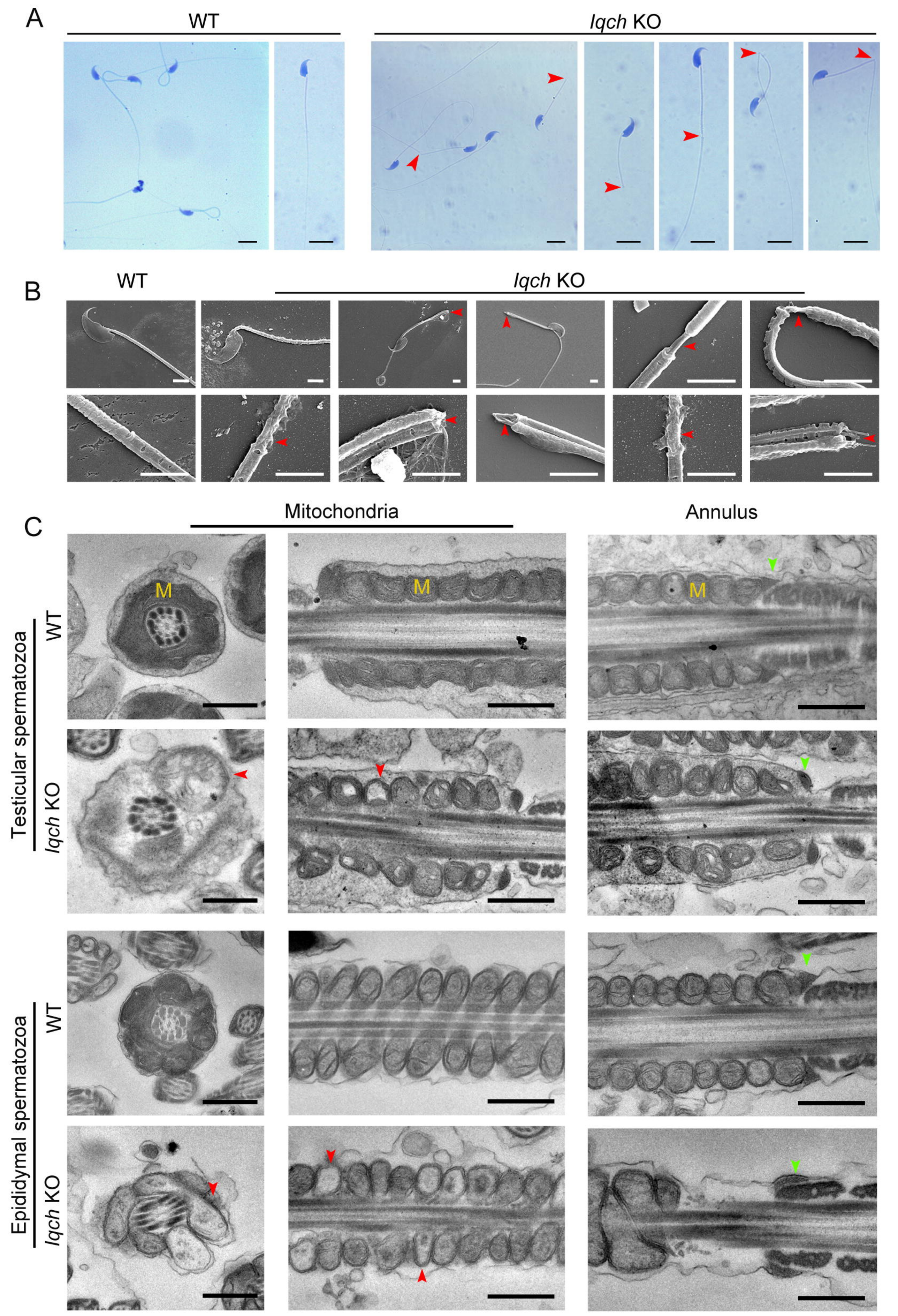
A
WT
Iqch KO
B
WT
Iqch KO
C
Mitochondria
Annulus
Testicular spermatozoa
WT
Iqch KO
Epididymal spermatozoa
WT
Iqch KO
M
M
M

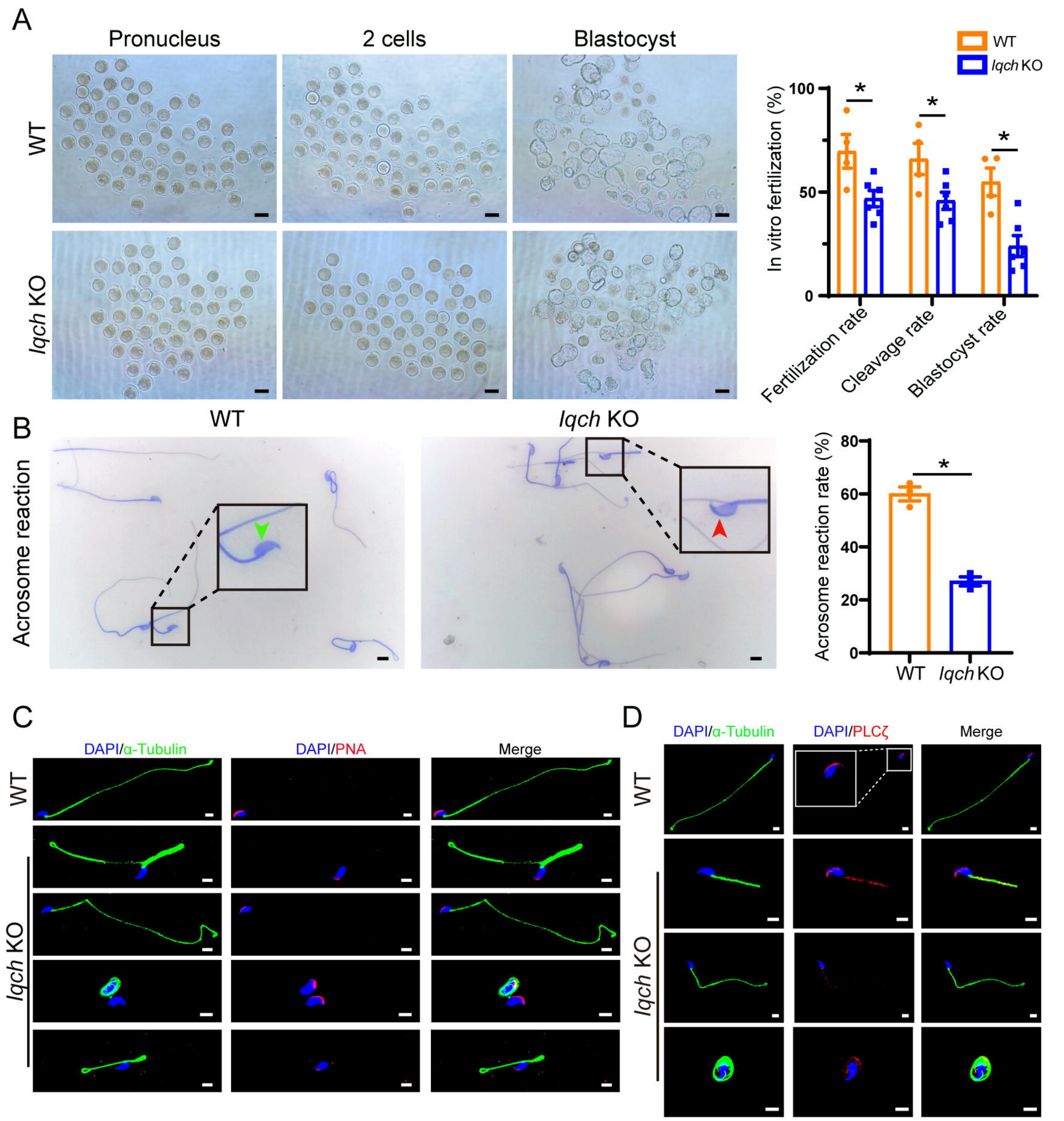
A
Pronucleus
2 cells
Blastocyst
WT
lqch KO
WT
lqch KO
In vitro fertilization (%)
100
50
0
*
*
*
Fertilization rate
Cleavage rate
Blastocyst rate
B
WT
lqch KO
Acrosome reaction
Acrosome reaction rate (%)
80
60
40
20
0
*
WT
lqch KO
C
DAPI/α-Tubulin
DAPI/PNA
Merge
WT
lqch KO
D
DAPI/α-Tubulin
DAPI/PLCζ
Merge
WT
lqch KO

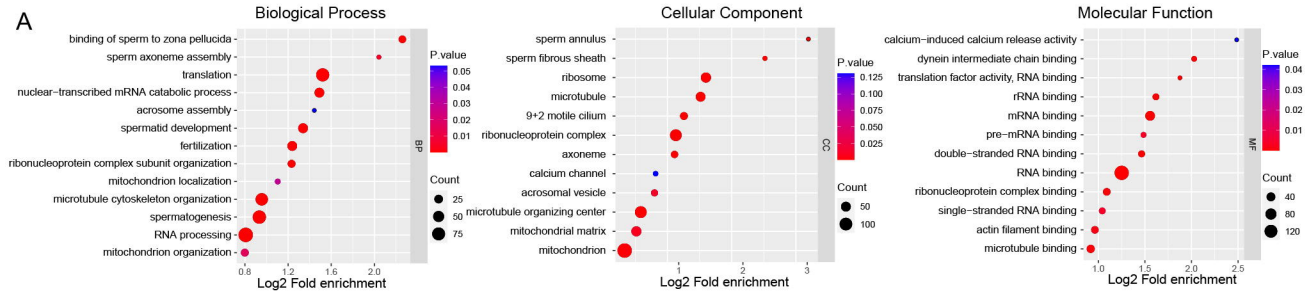

B

Protein accession	Protein names	Gene names	Protein score
Q9D8E6	60S ribosomal protein L4	Rpl4	221
P47911	60S ribosomal protein L6	Rpl6	196
P14148	60S ribosomal protein L7	Rpl7	164
P47963	60S ribosomal protein L13	Rpl13	143
Q9CR57	60S ribosomal protein L14	Rpl14	109
P62908	40S ribosomal protein S3	Rps3	97
Q6ZWN5	40S ribosomal protein S9	Rps9	96
P35980	60S ribosomal protein L18	Rpl18	91
P27659	60S ribosomal protein L3	Rpl3	83
P62264	40S ribosomal protein S14	Rps14	83
P12970	60S ribosomal protein L7a	Rpl7a	73
P14131	40S ribosomal protein S16	Rps16	73
P19253	60S ribosomal protein L13a	Rpl13a	72
P62702	40S ribosomal protein S4, X isoform	Rps4x	66
P62301	40S ribosomal protein S13	Rps13	65
P47915	60S ribosomal protein L29	Rpl29	63
P14115	60S ribosomal protein L27a	Rpl27a	62
P61255	60S ribosomal protein L26	Rpl26	60
P84099	60S ribosomal protein L19	Rpl19	58
P25444	40S ribosomal protein S2	Rps2	53
P47962	60S ribosomal protein L5	Rpl5	53
Q9CPR4	60S ribosomal protein L17	Rpl17	51
P62754	40S ribosomal protein S6	Rps6	48
P14869	60S acidic ribosomal protein P0	Rplp0	47
P62751	60S ribosomal protein L23a	Rpl23a	47
P60867	40S ribosomal protein S20	Rps20	47
O09167	60S ribosomal protein L21	Rpl21	44
Q9CZM2	60S ribosomal protein L15	Rpl15	42
P35979	60S ribosomal protein L12	Rpl12	42
P97351	40S ribosomal protein S3a	Rps3a	36
P62855	40S ribosomal protein S26	Rps26	35
P62082	40S ribosomal protein S7	Rps7	34
P62849	40S ribosomal protein S24	Rps24	32

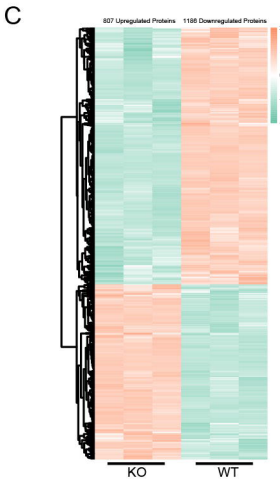

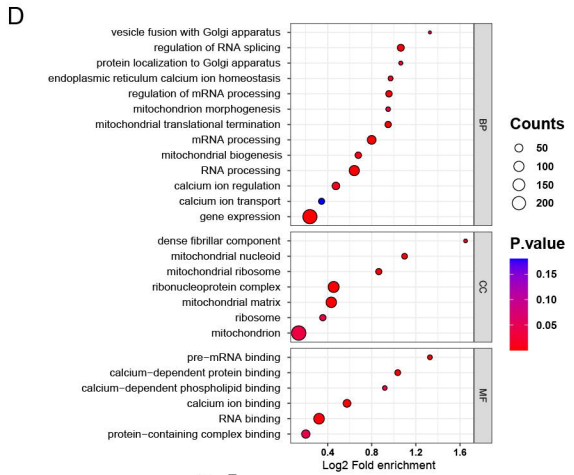

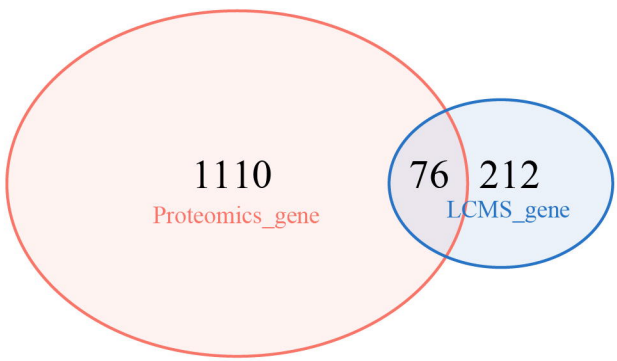

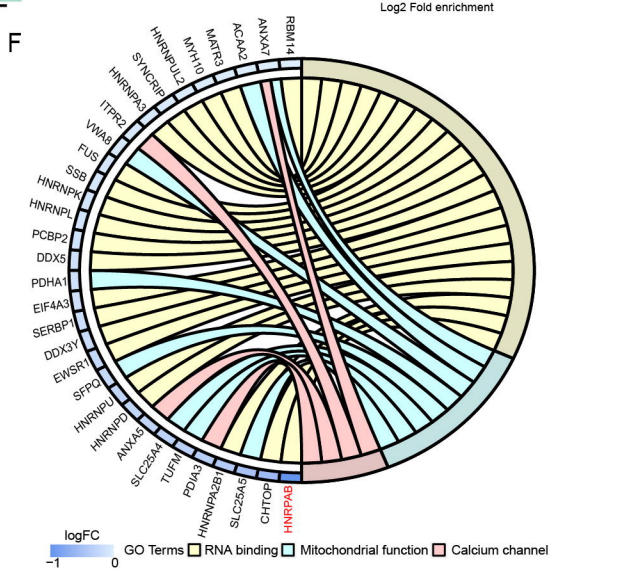

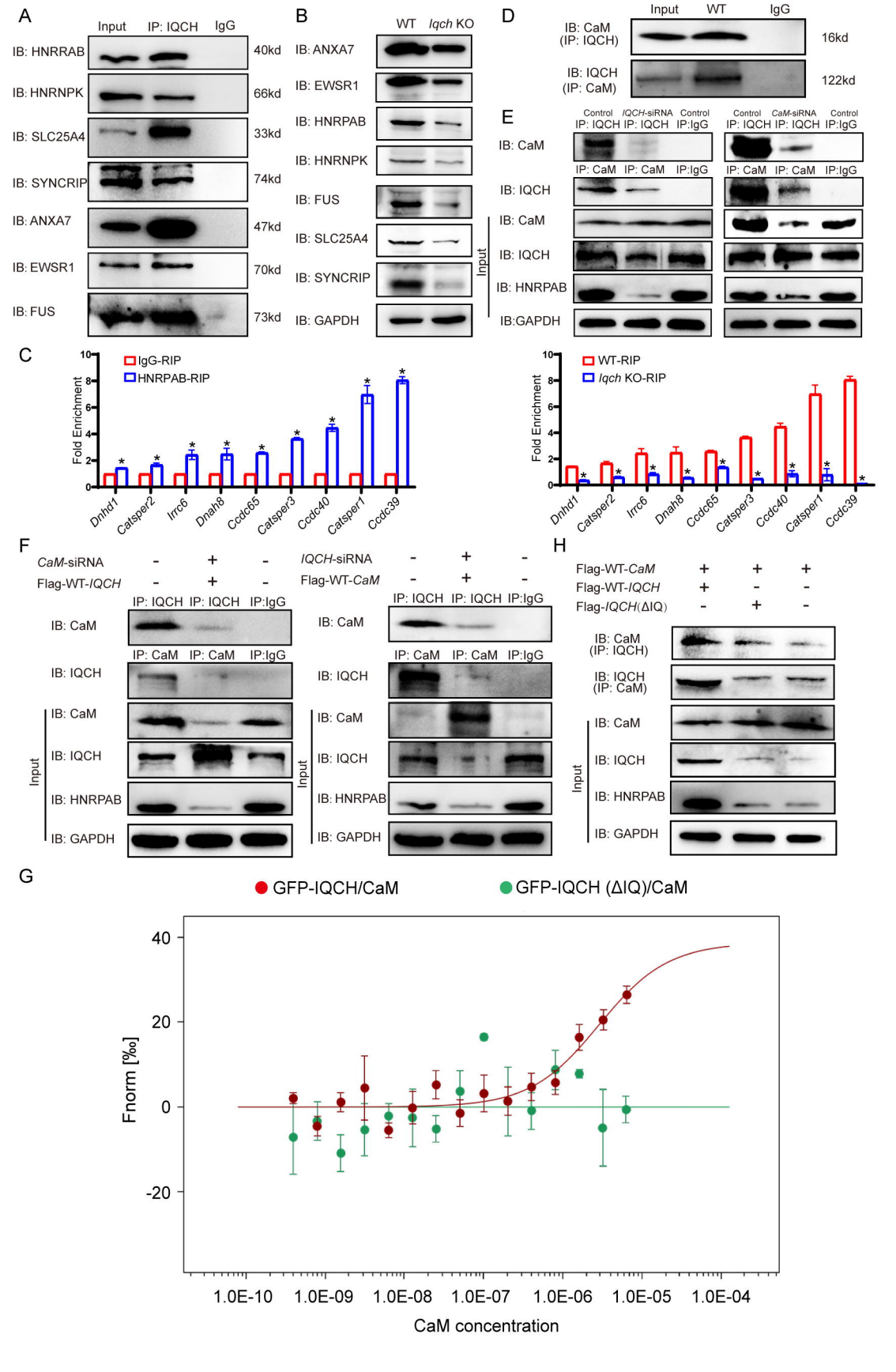
A
Input
IP: IQCH
IgG
IB: HNRRAB
40kd
IB: HNRNPK
66kd
IB: SLC25A4
33kd
IB: SYNCRIP
74kd
IB: ANXA7
47kd
IB: EWSR1
70kd
IB: FUS
73kd
B
WT
Iqch KO
IB: ANXA7
IB: EWSR1
IB: HNRPAB
IB: HNRNPK
IB: FUS
IB: SLC25A4
IB: SYNCRIP
IB: GAPDH
Input
D
Input
WT
IgG
IB: CaM (IP: IQCH)
16kd
IB: IQCH (IP: CaM)
122kd
E
Control
IQCH-siRNA
Control
IP: IQCH
IP: IQCH
IP:IgG
CaM-siRNA
IP: CaM
IP: CaM
IP:IgG
IB: CaM
IB: IQCH
IB: HNRPAB
IB:GAPDH
C
IgG-RIP
HNRPAB-RIP
Fold Enrichment
Dnhd1
Catsper2
Irrc6
Dnah8
Ccdc65
Catsper3
Ccdc40
Catsper1
Ccdc39
WT-RIP
Iqch KO-RIP
F
CaM-siRNA
Flag-WT-IQCH
IQCH-siRNA
Flag-WT-CaM
IP: IQCH
IP:IgG
IP: CaM
IB: CaM
IB: IQCH
IB: HNRPAB
IB: GAPDH
Input
H
Flag-WT-CaM
Flag-WT-IQCH
Flag-IQCH(ΔIQ)
IB: CaM (IP: IQCH)
IB: IQCH (IP: CaM)
G
GFP-IQCH/CaM
GFP-IQCH (ΔIQ)/CaM
Fnorm [‰]
CaM concentration
1.0E-10
1.0E-09
1.0E-08
1.0E-07
1.0E-06
1.0E-05
1.0E-04

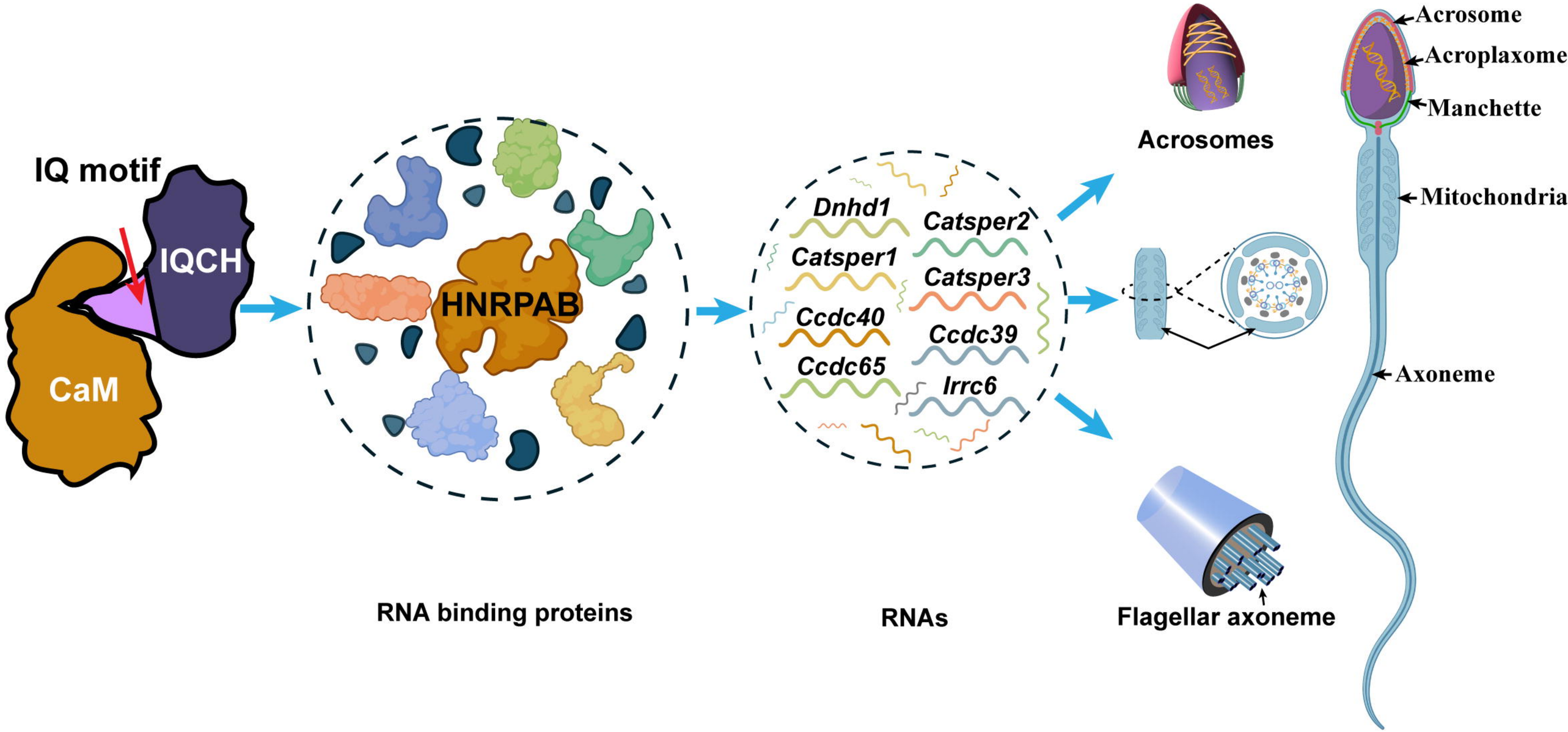
IQ motif
IQCH
CaM
HNRPAB
RNA binding proteins
Dnhd1
Catsper2
Catsper1
Catsper3
Ccdc40
Ccdc39
Ccdc65
Irrc6
RNAs
Acrosomes
Flagellar axoneme
Acrosome
Acroplaxome
Manchette
Mitochondria
Axoneme